WARWICK
THE UNIVERSITY OF WARWICK

Manuscript version: Author's Accepted Manuscript
The version presented in WRAP is the author's accepted manuscript and may differ from the published version or Version of Record.

Persistent WRAP URL:
http://wrap.warwick.ac.uk/89792

How to cite:
Please refer to published version for the most recent bibliographic citation information. If a published version is known of, the repository item page linked to above, will contain details on accessing it.

Copyright and reuse:
The Warwick Research Archive Portal (WRAP) makes this work by researchers of the University of Warwick available open access under the following conditions.

Copyright © and all moral rights to the version of the paper presented here belong to the individual author(s) and/or other copyright owners. To the extent reasonable and practicable the material made available in WRAP has been checked for eligibility before being made available.

Copies of full items can be used for personal research or study, educational, or not-for-profit purposes without prior permission or charge. Provided that the authors, title and full bibliographic details are credited, a hyperlink and/or URL is given for the original metadata page and the content is not changed in any way.

Publisher's statement:
Please refer to the repository item page, publisher's statement section, for further information.

For more information, please contact the WRAP Team at: wrap@warwick.ac.uk.

warwick.ac.uk/lib-publications

Electrochemical Reduction of CO_2 with an Oxide-Derived Lead Nano-Coralline Electrode in Dimcarb

Lu Chen,[a] Fengwang Li,[a] Cameron L. Bentley,[b] Mike Horne,[c]

Alan M. Bond,[a] and Jie Zhang*[a]

[a]School of Chemistry and ARC Centre of Excellence for Electromaterials Science, Monash University, Clayton, Vic 3800, Australia

[b]Department of Chemistry, University of Warwick, Coventry, CV4 7AL, U.K.

[c]CSIRO Minerals Resources Flagship, Clayton, Vic 3168, Australia

Abstract

Electro-reduction of CO_2 in the distillable ionic liquid dimethylammonium dimethylcarbamate (dimcarb) has been investigated with an oxide-derived lead (od-Pb) electrode. Compared with unmodified polycrystalline Pb, where H_2 is the dominant electrolysis product, od-Pb possesses impressive catalytic properties for the reduction of CO_2 in dimcarb (mixing molar ratio of CO_2 and DMA > 1: 1.8), with faradaic efficiencies for the generation of H_2, CO and $[HCOO]^-$ of approximately 15%, 10% and 75%, respectively. These efficiencies are independent of the applied potential in the range -1.34 to -3.34 V vs $Cc^{+/0}$ (where Cc^+ = cobaltocenium). Thorough analysis of the properties of od-Pb demonstrate that its intrinsically high catalytic activity towards CO_2 reduction compared to bulk Pb is attributable to increased surface roughness and greater surface area (*ca.* 10 times higher), rather than the existence of residual metal oxides that is known to suppress the Hydrogen evolution reaction, preferred crystal orientation or the existence of metastable active sites.

Introduction

Global usage of fossil fuels in energy-related applications has led to elevated atmospheric carbon dioxide (CO_2) levels, which has resulted in a number of contemporary environmental issues. [1] For this reason, the conversion of CO_2 to energy-rich fuels or other useful chemicals is being vigorously studied. Electrochemical reduction has been shown to be a promising method for this purpose, [2] because the driving force for the CO_2 reduction reaction can be readily controlled through the applied potential. Currently, the main challenges associated with the electrochemical conversion of CO_2 are the high overpotential required to drive the reduction reaction, particularly the initial one electron transfer process to form the $CO_2^{\cdot-}$ radical intermediate, the low faradaic efficiencies (FE) for product formation and poor product selectivity. [3] A productive way to address these challenges is to carefully select electro-catalysts for the reduction and to date, the most widely used materials in this application are the transition/post-transition metals and their compounds (*i.e.*, oxides or complexes). [2b]

In addition to the catalyst, the solvent and electrolyte must also be considered when designing an electrochemical CO_2 reduction system. Three categories of solvent; aqueous [4], non-aqueous [5] and ionic liquids (ILs) have shown promise as CO_2 conversion media and each has distinct advantages and disadvantages. ILs are considered particularly attractive for CO_2 reduction because certain ILs are useful solvents, electrolytes and catalysts [3b, 3c, 6] Despite their potential utility, the application of ILs for electrochemical CO_2 conversion on an industrial scale is hindered by their comparatively high cost and the difficulties associated with product separation/recovery of the reaction medium after electrolysis.

In a previous study [7], we proposed the relatively cheap and distillable amine-based IL, dimethylammonium dimethylcarbamate (dimcarb), as a medium for electrochemical conversion of CO_2. Importantly, and unlike conventional aprotic ILs, dimcarb can be easily recovered by distillation at approximately 60 °C, at which temperature it breaks down into its constituents: dimethylamine (Me_2NH or DMA) and CO_2. In a practical (electrochemical) context, this means that after bulk electrolysis, the unreacted dimcarb can be readily recycled. Additionally, the medium simultaneously functions as the CO_2 and proton source, as well as solvent and supporting electrolyte, which significantly simplifies the operational requirements. It is these unique properties that allow dimcarb to effectively act as an electrochemical CO_2 conversion medium. Dimcarb can be readily synthesized by mixing solid CO_2 (dry ice) and DMA gas at a molar ratio of 1:1.8, according to the reactions given in Equations (1) and (2).

$$CO_{2(g)} + Me_2NH_{(g)} \rightleftharpoons Me_2NCOOH \quad (1)$$

$$Me_2NCOOH + Me_2NH_{(g)} \rightleftharpoons [Me_2NH_2]^+ + [Me_2NCOO]^- \quad (2)$$

The mixing ratio can be further varied between 1:1.6 and 1:1.9 by bubbling with CO_2 or DMA, respectively, post-synthesis. [8] Notably, these practical mixtures in the 1:1.6 to 1:1.9 ratio range are all 'CO_2 rich' compared with the stoichiometric ratio of 1:2, a desirable factor that assists with the reduction reaction.

In our previous study [7], 17 different metals were screened for their electro-catalytic activity towards CO_2 reduction in dimcarb and, of the metals investigated, indium(In), tin(Sn), zinc(Zn), gold(Au) and silver(Ag) were shown to be the most promising for this application. In addition, we showed that introducing additional CO_2 into the medium, improves the catalytic performance of all these metals. In all cases, the

hydrogen evolution reaction (HER) competed most strongly, decreasing the FE for CO_2 reduction whenever it occurred. It follows that, in order to improve the performance of electro-catalysts in this application, new materials need to be designed which suppress the HER while maintaining activity towards CO_2 reduction.

A number of research groups have reported promising results when using so-called "oxide-derived" metallic catalysts for the electrochemical CO_2 reduction. For example, oxide-derived copper(Cu)[9], Au[10], Sn[11], lead(Pb)[12], Ag[13], bismuth(Bi)[14] and cobalt(Co)[15] have all been shown to possess enhanced electro-catalytic activity towards CO_2 reduction compared with the unmodified bulk (polycrystalline) metal in aqueous bicarbonate media. In order to generate an oxide-derived metal from a polycrystalline foil, an oxide-surface layer needs to be generated by electrochemical anodization in acidic/alkaline aqueous solution or thermal oxidation in air and then subsequently electrochemically converted back into metal (now termed an 'oxide-derived' metal).

We expand upon our previous work [7] by investigating the application of oxide-derived metal electrodes of In, Bi, Sn and Pb as electro-catalysts for CO_2 reduction in dimcarb. In previous study, we have demonstrated that the HER is the main side-reaction during CO_2 conversion with flat metals. Therefore, in order to improve the faradaic efficiency for CO_2 reduction, the HER needs to be suppressed. In this study, we found that the HER can be suppressed using oxide-derived porous electrodes, including In, Bi, Sn and Pb. However, oxide-derived porous Pb electrode shows the highest improvement among all. (Figure S1) Therefore, it was chosen for a detailed investigation.

In this study, the distribution of electrolysis products is reported as a function of applied potential, with the analyses being performed by gas chromatography for H_2 and CO determination and NMR for formate determination.

Experimental Section

Reagents

The chemicals used and their sources are listed below. In all cases, they were used without further purification. Dimethylamine (Me_2NH, 99%), hydrogen (H_2, Standard Reference Gas), carbon monoxide (CO, Standard Reference Gas), lead chloride (98%), cobaltocenium hexafluorophosphate ($[Cc]^+[PF_6]^-$, 98%), dimethyl fumarate (97%) and deuterochloroform ($CDCl_3$, 99%) were from Sigma-Aldrich, while nitrogen (N_2, 99.999%) helium (He, 99.9%) and carbon dioxide (CO_2, 99.9%, Aligal) were from Air Liquide, Australia. The lead (Pb) foil was purchased from Zr-industrial, Shanghai, China with a purity of 99.9%. Dimethylammonium dimethylcarbamate was synthesized as per literature procedures. [16]

Electrochemical systems and procedures

All dc cyclic voltammetric and (potentiostatic) bulk electrolysis experiments were carried out at room temperature (22 ± 2°C) using a standard three-electrode cell with a CHI760D electrochemical workstation (CHI Instruments, Austin, Texas, USA). Unless otherwise stated, Pb or od-Pb was used as the working electrode (cathode) and platinum foil as the counter electrode (anode). Preparation of the od-Pb working electrodes is described below. The quasi-reference electrode consisted of a small, fritted glass tube containing a silver wire in contact with neat dimcarb. The reference electrode potential was stable within a few mV on the bulk electrolysis timescale, and was calibrated against the $Cc^{+/0}$ process, post electrolysis.

Fourier transformed alternating current (FTAC) voltammetric measurements were carried out with an instrument built in-house [17] and using a sine wave perturbation (amplitude 80 mV and frequency 9.02 Hz) superimposed onto a dc ramp (scan rate of 44.7 mV s^{-1}). A power spectrum was then obtained by applying Fourier

transformation on the total current resulting from this applied potential waveform. After the frequency band of interest was selected, inverse Fourier transformation was used to generate the desired aperiodic dc or ac harmonic components. [17-18]

Bulk electrolysis was conducted in a gas-tight H-shape electrolysis cell under a CO_2 or DMA atmosphere, where a porous glass frit separated the anodic and cathodic half-cells. High purity CO_2 or DMA gas was introduced to remove oxygen prior to electrochemical measurements. After bubbling for approximately 10 minutes, the electrolysis cell was sealed tightly with a rubber stopper.

Microscopic and spectroscopic characterization techniques

Surface morphologies of representative electrodes were imaged using a Magellan 400 FEGSEM scanning electron microscope (SEM). Powder X-ray Diffraction (PXRD) data were collected with a Bruker D2 X-ray powder diffractometer (Cu $K_{\alpha 1}$ radiation) using a scan rate of 0.5 degree per minute and a step increment of 0.02 degree per step.

Product analysis

An Agilent (7820 A) Gas Chromatography (GC) system, equipped with a HP-plot molesieve (5Å) column and a thermal conductivity detector (TCD) was used to identify gaseous products present in the headspace. In order to achieve adequate peak separation, a shorter column with a carrier gas of He was used when detecting CO and a longer column with a carrier gas of N_2 was used to detect H_2. Calibration curves for H_2 and CO were constructed by injecting a known amount of pure H_2 and CO and plotting the peak area against the amount injected. The detailed analysis process was reported in an earlier study. [7] It needs to be noted that, in some cases, the total faradaic efficiencies slightly exceed the theoretical limitation of 100%, this is mainly

attributed to the experimental uncertainty associated with determination of the product concentrations.

Results and Discussion

In the following sections, unless otherwise stated, the molar mixing ratio of CO_2 and DMA is > 1:1.8, as this dimcarb composition showed the most promising results in our previous study. [7] "Single treated od-Pb" and "double treated od-Pb" refers to od-Pb that was obtained from flat Pb after one and two thermal oxidation/electrochemical reduction treatment cycle(s) (detailed below), respectively.

Cyclic Voltammetry in Dimcarb with a PbO coated Pb electrode

Cyclic voltammetric experiments were carried out in dimcarb using a PbO coated Pb electrode generated by exposing Pb foil to air at 220 °C for 24 hours. A typical voltammogram is shown in Figure 1. The initial potential was set to the open circuit value, where no faradaic processes occur. The potential was scanned in the negative direction immediately after the initial potential was chosen to avoid the dissolution of PbO in Dimcarb to a significant extent. The peak located at -0.2 V vs $Cc^{0/+}$ is attributed to the reduction of PbO (supported by the PXRD measurements shown below in Figure 2a), which is thought to occur via the mechanism shown in Eq. 3, as $[Me_2NH_2]^+$ is the strongest acid present in dimcarb. [7]

$$PbO + 2[Me_2NH_2]^+ + 2e^- \rightarrow Pb + 2Me_2NH + H_2O \quad (3)$$

Upon sweeping to further negative potentials, an almost linear increase in the reduction current with potential is observed. This linear current-potential behavior is also observed with the untreated polycrystalline metals, and is due to the effects of

ohmic polarization (*i.e.*, IR_u drop), especially when the current density is high, since the conductivity of dimcarb is relatively low at room temperature (1.7 mS cm^{-1} at 293 K). [19] The current fluctuations seen in the cyclic voltammogram at high current densities (see Figure 1) are caused by the generation and detachment of gas bubbles that are visible to the naked eye on the metal surface.

In conventional organic solvent electrolyte media, the electro-catalytic performance of an electrode material towards CO_2 reduction can be studied by undertaking control experiments under N_2 atmospheres where reactive CO_2 species are absent. Unfortunately, such an approach cannot be adopted in dimcarb, since it intrinsically contains CO_2, which means that the information that can be obtained from cyclic voltammetry is very limited. Therefore, the electro-catalytic performance of od-Pb towards CO_2 reduction was evaluated by analysing the electrolysis products produced under potentiostatic conditions, as explained in detail below.

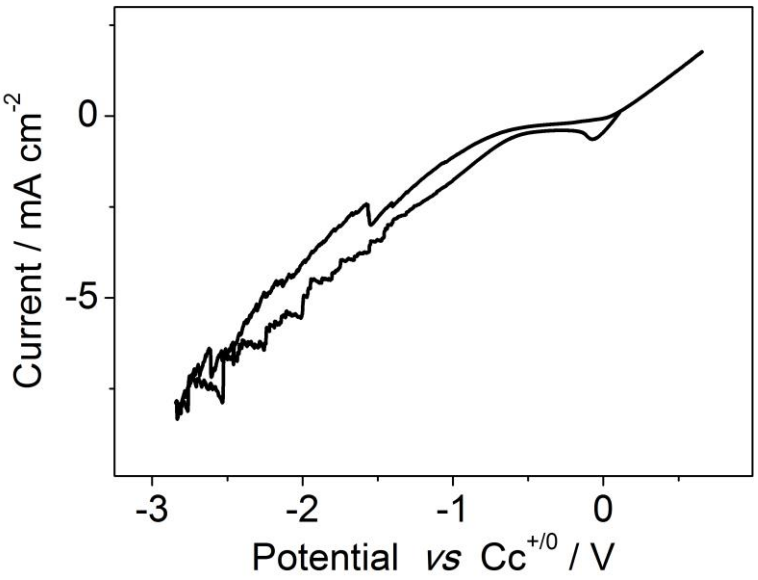

Figure 1. A cyclic voltammogram obtained at a PbO coated Pb electrode in dimcarb at a scan rate of 0.1 V s^{-1}.

Optimization of od-Pb for CO_2 reduction in dimcarb

The synthesis of the oxide-derived Pb (od-Pb) involves two steps: the initial thermal oxidation of Pb to PbO and the subsequent electrochemical reduction of PbO to metallic od-Pb. Several control experiments were performed to optimize each of these steps.

Influence of the PbO layer thickness.

Polycrystalline Pb was oxidized using three different conditions to generate PbO surface layers of different thicknesses. These conditions were: (i) exposure to air at room temperature for 1 month; (ii) exposure to air at 220 °C for 2 hours and; (iii) exposure to air at 220 °C for 24 hours. The phase composition of the surface oxide layer on each of the samples was characterized by PXRD, as shown from Figure 2a(i) to Figure 2a(iii). In all three cases, the only oxide detected was PbO and the magnitudes of the peaks associated with PbO increase with the intensity of the oxidative treatment (room temperature, 1 months < 220°C, 2 hours < 220°C, 24 hours), an observation attributed to an increase in the thickness of the PbO layer.

In order to understand the influence of the thickness of the precursor PbO layer on the catalytic properties of the resultant od-Pb, three samples prepared as described above were electrochemically reduced at -3.34 V vs $Cc^{0/+}$ for 4 hours to convert PbO to metallic od-Pb. As shown in Figure 2a(iv), only a very small trace of the PbO peaks remain in the od-Pb PXRD patterns after the reduction. This residual PbO peaks most likely arise from exposure of the od-Pb to the air during sample transfer for PXRD measurements. In order to evaluate the catalytic properties of the three od-Pb samples, they were used as cathodes in bulk electrolysis carried out at -2.84 V vs $Cc^{0/+}$ in dimcarb. The resultant product distribution is summarized in Figure 2(b). Compared with the flat Pb, all three od-Pb electrodes show increased catalytic performance and

the od-Pb synthesized from the Pb electrode with the thickest PbO layer (*i.e.*, 220°C, 24 hours) possesses the highest catalytic activity for the reduction of CO_2 to $[HCOO]^-$ in dimcarb, with FEs for the generation of H_2, CO and $[HCOO]^-$ of 34.4%, 10.0% and 62.4%, respectively.

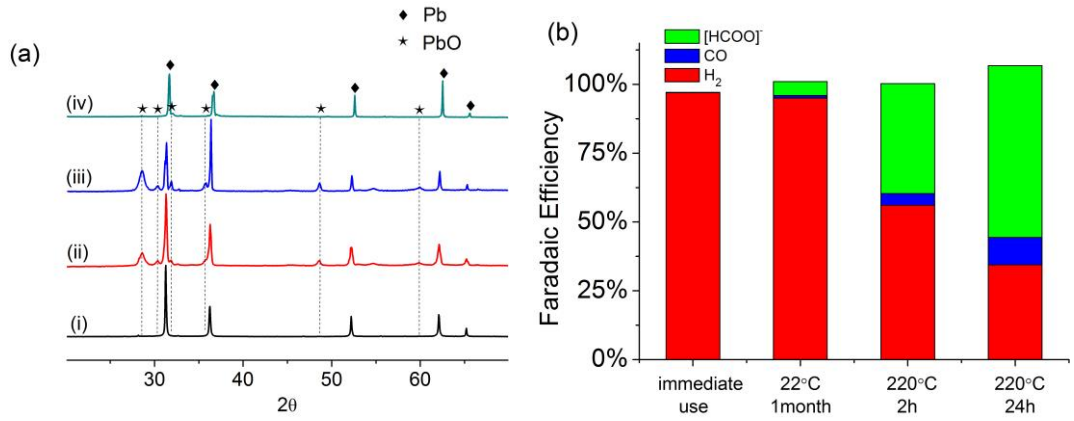

Figure 2. (a) PXRD patterns of Pb foil samples treated as follows: (i) exposure to air at room temperature for 1 month (22°C, 1 month); (ii) exposure to air at 220 °C for 2 hours (220°C, 2 h) and; (iii) exposure to air at 220 °C for 24 hours (220°C, 24 h); (iv) od-Pb prepared by electrochemically reducing oxidised foils at -3.34V vs. $Cc^{0/+}$ for 4 hours. (b) FEs calculated for each Pb foil sample from analysis of the electrolysis products after bulk electrolysis in dimcarb at an applied potential of -2.84 V vs. $Cc^{+/0}$.

Finally, it is generally well known that the thickness of a metal oxide surface layer will not increase above a well-defined 'plateau' value predicted by the parabolic rate law for the oxidation of metals [20], implying extended oxidative treatments are not useful. This limit was observed here, as shown in Figure 2(a), in which the PbO peak intensities change by only small amounts when the oxidation time at 220°C is increased from 2 hours to 24 hours. Increasing the oxidation time above 24 hours had a negligible influence on the thickness of the metal oxide (PbO) layer. For this reason, the oxidative pretreatment protocol used in all subsequent experiments was exposure to air at 220°C for 24 hours. It should be noted that similar phenomenon has previously been reported, [9a, 21] where a certain "threshold thickness" of metal oxide (*e.g.*, Cu_2O or AuO_x) was required to produce a stable and efficient electro-catalyst.

Influence of the applied potential during pre-reduction of PbO.

As shown in Figure 1, the voltammetric peak attributed to PbO reduction occurs at a potential of *ca.* -0.2 V vs $Cc^{0/+}$. However, long pre-reduction times at potentials significantly more negative than -0.2 V vs $Cc^{0/+}$ were required to produce od-Pb with favorable CO_2 reduction characteristics. For example, od-Pb electrodes made by applying pre-reduction potentials in the range -1.34 V vs $Cc^{0/+}$ to -2.34 V vs $Cc^{0/+}$ for between 0.5 and 4 hours show poor reproducibility in terms of the reduction product distribution produced during bulk electrolysis. Nevertheless, more negative pre-reduction potentials produce more favorable product distributions (*i.e.*, a decrease in the FE for H_2) and improve the reproducibility of the results. For these reasons, in order to guarantee high CO_2 reduction efficiency and high reproducibility, the pre-reduction protocol was selected to be -3.34 V vs $Cc^{0/+}$ for 4 hours.

In order to determine why more negative pre-reduction potentials result in od-Pb with more favorable electro-catalytic properties, the electrodes were characterized using SEM, as shown in Figure 3. The potentials selected for reduction of PbO fall into two categories: (i) -0.24 V vs $Cc^{0/+}$, where only the reduction of PbO occurs, and (ii) -1.34 V vs $Cc^{0/+}$, -2.34 V vs $Cc^{0/+}$ or –3.34 V vs $Cc^{0/+}$, where both the reduction of PbO and the HER occur simultaneously (see Figure 1). The micrographs in Figure 3 show the od-Pb obtained at the three most negative applied potentials (3(c) to 3(f)) possess the highest surface roughness. Moreover, the average size of the surface features decreases as the applied potential becomes more negative. This is because when held at extremely negative applied potentials, the generation of hydrogen bubbles occurs simultaneously with PbO reduction (see Eq. 3), a process that alters the surface morphology of the soft Pb electrode.

In summary, the process of making od-Pb electrodes with good electro-catalytic performance toward CO_2 reduction in dimcarb was optimized and the procedure chosen is as follows.

1. Thermal oxidation at 220 °C for 24 hours.
2. Pre-reduction at -3.34 V vs. $Cc^{0/+}$ for 4 hours.

All od-Pb was synthesized in this manner, unless otherwise stated.

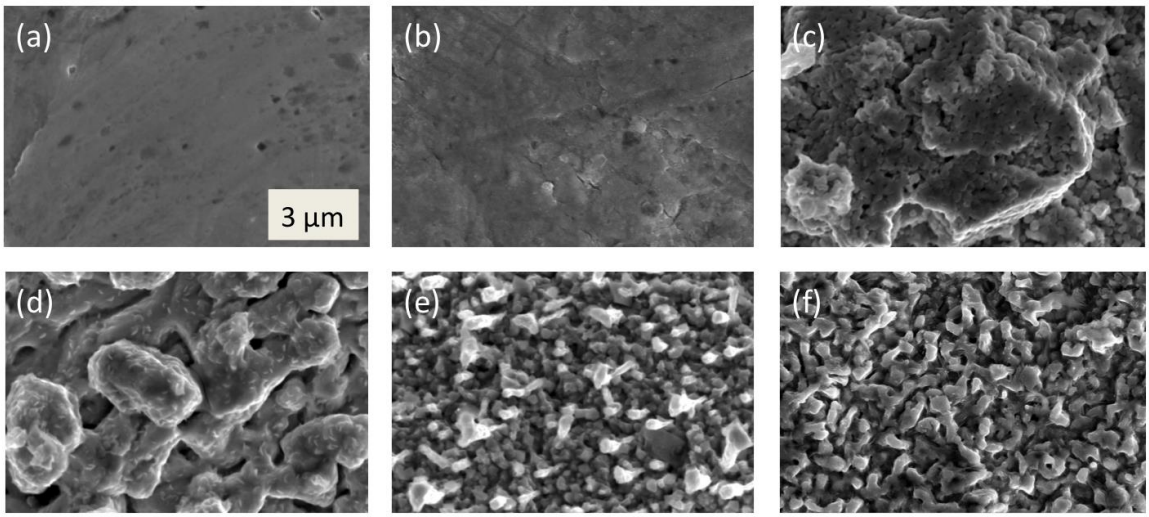

Figure 3. SEM micrographs of: (a) unmodified Pb foil; (b) Pb foil which has been oxidized in the air at 220 °C for 24 hours; and od-Pb samples obtained by reducing PbO coated Pb at (c) -0.24 V vs $Cc^{0/+}$ for 4 hours; (d) -1.34 V vs $Cc^{0/+}$ for 4 hours; (e) -2.34 V vs $Cc^{0/+}$ for 4 hours, and (f) –3.34 V vs $Cc^{0/+}$, 4 hours. All micrographs have the same scale bar, as shown in (a).

Bulk electrolysis with od-Pb in dimcarb

Bulk electrolyses carried out in dimcarb using od-Pb cathodes fabricated by the optimized protocol outlined above generated product distributions that varied with the applied potential, as summarized in Table 1. Comparison of these results with those reported previously [7] shows that the HER is significantly inhibited when od-Pb cathodes are used in place of unmodified, polycrystalline Pb cathodes. It is also worth noting that the distributions of the reduction products do not vary significantly with applied potential in the range -1.34 to -3.34 V vs. $Cc^{+/0}$; the FE for the generation of H_2,

CO and $[HCOO]^-$ on od-Pb are around 30%, 10% and 60%, respectively. The reason for this is discussed in our previous study on electrochemical CO_2 reduction in dimcarb with unmodified polycrystalline metal electrodes. The partial current densities for generating H_2, CO and $[HCOO]^-$ are around 8.0, 3.0 and 16.8 mA cm^{-2} respectively at potential of -3.34 V vs $Cc^{0/+}$.

Table 1. Product distributions following bulk electrolyses at different potentials on od-Pb cathodes in dimcarb.

Electrolysis Potential / V	Faradaic Efficiency			
	H_2	CO	$[HCOO]^-$	Sum
-1.34	30.3%	7.5%	59.8%	97.6%
-1.84	31.0%	10.0%	62.4%	103.4%
-2.34	27.8%	10.5%	58.0%	96.3%
-2.84	31.0%	10.4%	59.7%	101.1%
-3.34	30.8%	10.4%	57.9%	99.1%

Bulk electrolysis with double and triple treated od-Pb

Following bulk electrolysis using an od-Pb cathode with a surface morphology similar to that shown in Figure 3(f), the electrode was thermally oxidized a second time at 220 °C for 24 hours in order to generate a thicker PbO layer, as shown in Figure 4(a). The thicker PbO layer was subsequently reduced using the same protocol as before: -3.34 V vs $Cc^{0/+}$ for 4 hours to generate double treated od-Pb, Figure 4(b). Comparing Figure 3(f) with Figure 4(b) suggests there is no observable difference between the surface morphologies of the single treated and double treated od-Pb electrodes. It is expected that the od-Pb layer shown in Figure 4(b) will be thicker than that shown in Figure 3(f). Unfortunately, direct measurements of the thickness of the layer by cross-sectional imaging with SEM are very difficult because the mechanical softness of Pb makes sample preparation extremely challenging. Changes in the surface roughness/area is explored in greater detail below.

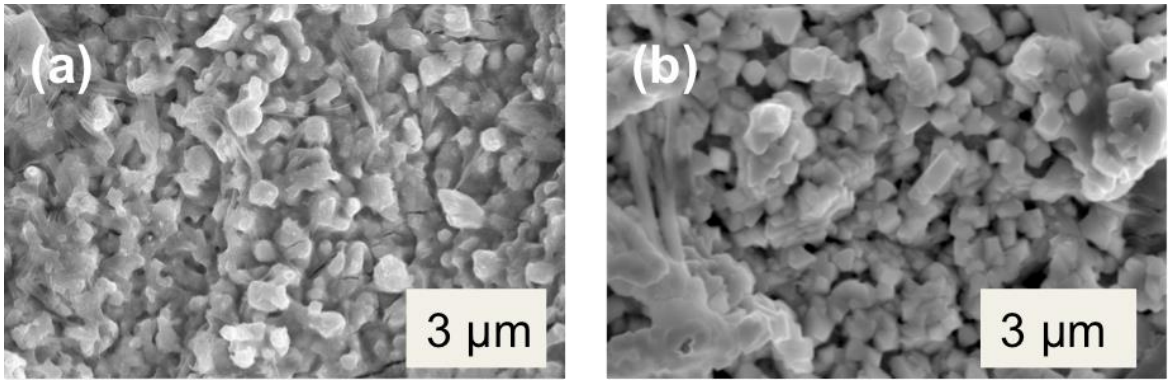

Figure 4. SEM micrographs of (a) the single treated od-Pb after re-oxidation in the air at 220 °C for 24 hours to get a thicker PbO layer and (b) electrochemical reduction of the surface shown in (b) at –3.34 V vs $Cc^{0/+}$ for 4 hours generates double treated od-Pb.

Table 2. Product distributions following bulk electrolyses at different potentials on double treated od-Pb cathodes in dimcarb.

Potential / V	Faradaic Efficiency			
	H_2	CO	$[HCOO]^-$	Sum
-1.34	18.5%	8.3%	78.7%	105.5%
-1.84	11.5%	11.6%	80.0%	103.1%
-2.34	14.0%	11.5%	71.9%	97.4%
-2.84	11.7%	8.9%	76.2%	96.8%
-3.34	22.6%	10.0%	71.5%	104.1%

Following synthesis, the catalytic activities of double treated od-Pb electrode for CO_2 reduction in dimcarb were evaluated by bulk electrolysis as described previously. The results are summarized in Table 2. By comparing Table 2 with Table 1, it is clear the catalytic performance of od-Pb is enhanced by the additional thermal oxidation/electrochemical reduction cycle. Faradaic efficiencies for the generation of H_2, CO and $[HCOO]^-$ on double treated od-Pb cathodes are approximately 15%, 10% and 75%, respectively. The partial current densities for generating H_2, CO and $[HCOO]^-$ are around 5.7, 2.5 and 17.8 mA cm^{-2} respectively at potential of -3.34 V vs $Cc^{0/+}$.

Re-treating double treated od-Pb to make triple treated od-Pb cathodes does not produce any further improvements in the product distribution. Finally, in order to assess the stability of the od-Pb/dimcarb system, bulk electrolysis was carried out for 24 hours with the double treated od-Pb electrode, and the product distribution was periodically evaluated. This distribution varied very little over the 24 hours period, indicating that the od-Pb/dimcarb CO_2 reduction system is likely to be stable during long-term electrolysis.

Double treated od-Pb is a far more effective catalyst for CO_2 reduction in dimcarb than is polycrystalline Pb foil. Under optimal conditions, Faradaic efficiencies for the generation of H_2, CO and $[HCOO]^-$ on this material are approximately 15%, 10% and 75%, respectively. From a practical perspective, the gaseous products could be used directly as syngas, since the ratio of H_2 and CO is within the syngas ratio, and the major product, $[HCOO]^-$ can be easily extracted from the reaction mixture by distillation to remove dimcarb. Our preliminary attempt on the laboratory scale achieved a distillation yield of over 80% after re-distillation of the unreacted dimcarb at 35 °C under vacuum.

CO_2 reduction on od-Pb in dimcarb with a mixing molar ratio < 1:1.8 (CO_2: DMA)

During extended reductive electrolysis in dimcarb, the consumption of CO_2 will gradually perturb the dynamic equilibria within this solvent (see Eqs. 1 and 2). In order to study whether this perturbation affects the catalytic performance of od-Pb, bulk electrolyses were carried out in dimcarb in which the mixing molar ratio of CO_2 and DMA was < 1:1.8. The product distribution recorded at different applied potentials is summarized in Table 3. Clearly, as the ratio of CO_2 to DMA decreases, the electro-

catalytic activity of od-Pb towards CO_2 reduction is hindered, and H_2 becomes the sole electrolysis product at all applied potentials. This is not surprising, since an increase in the DMA concentration also increases the concentration of available protons associated with acidic species such as $[Me_2NH_2]^+$. Conversely, the concentration of free CO_2, the reactive CO_2 species present in dimcarb, is expected to diminish, due to the formation of the carbamate $[Me_2NCOO]^-$ (see Eqs. 1 and 2). It needs to be noted that the determination of $[HCOO]^-$ was not undertaken since H_2 is the dominant product with faradaic efficiency over 92%. The proposed mechanism(s) of the HER and CO_2 reduction reaction in dimcarb are discussed in detail in our previous work. For practical applications, this observation clearly illustrates the need for maintaining high CO_2 concentrations throughout the electrolysis.

Table 3. Product distribution following bulk electrolysis at different potentials at a double treated od-Pb electrode in dimcarb with mixing molar ratio < 1:1.8 (CO_2:DMA)				
Potential / V	Faradaic Efficiency			
	H_2	CO	$[HCOO]^-$	Sum
-1.34	92.8%	a	b	92.8%
-1.84	95.6%	a	b	95.6%
-2.34	95.3%	a	b	95.3%
-2.84	94.5%	a	b	94.5%
-3.34	96.0%	a	b	96.0%
a: negligible b: not determined				

Mechanistic studies

When the results discussed above (Tables 1 to 2) are compared with those collected in our previous work [7], it is evident that the identity of the electrolysis products are strongly dependent on the electrode material. When crystalline Pb is used as a cathode the HER dominates, whereas when od-Pb is used CO_2 reduction products (CO and formate) dominate. Similar behaviour has been observed with other oxide-derived metals in aqueous media, with the enhancement in electro-catalytic performance being attributed to one or more of the following factors:

(a) hindered HER due to the presence of surface oxides [15, 22],

(b) the presence of favourable crystal orientation [23] and/or

(c) the existence of metastable active sites. [9a, 10-11, 12]

Each of these factors is now considered in the context of the current study.

The existence of residual metal oxide (*e.g.*, PbO) on the od-Pb surface under bulk electrolysis conditions can be excluded for two reasons. Firstly, during the pre-reduction step, a very negative potential (-3.34 V vs $Cc^{0/+}$) and a long reduction time (4 hours) was used for reducing the oxide layer. This reduction potential is over 3 volts negative of the observed reduction potential for PbO in this solvent. Furthermore, the

PXRD pattern in Figure 2a(iv) indicates that there is no PbO residue (the small PbO peak is attributed to the exposure of od-Pb to air during sample preparation for PXRD). Secondly, even if there was a small amount of residual PbO at the surface it will dissolve and be reduced back to metallic Pb because dimcarb is a solvent with powerful coordinating ability. [16b] To test its solubility in dimcarb, solutions of PbO were successfully prepared with concentrations of up to 5 mM. Therefore, the presence of a residual PbO layer on the od-Pb can be ruled out.

The influence of favorable crystallographic orientations can also be excluded. PXRD patterns collected from four different samples of single treated od-Pb showed random orientation as judged from the relative peak intensities (Figure 5), even when prepared used the standard procedure: thermal oxidation in air at 220°C for 24 hours followed by electrochemical reduction at -3.34 V vs $Cc^{0/+}$ for 4 hours. Despite this, the four single treated od-Pb electrodes which gave rise to the XRD patterns shown in Figure 5 all performed similarly as electro-catalysts in dimcarb, indicating that there is no strong correlation between crystallographic orientation and electro-catalytic performance.

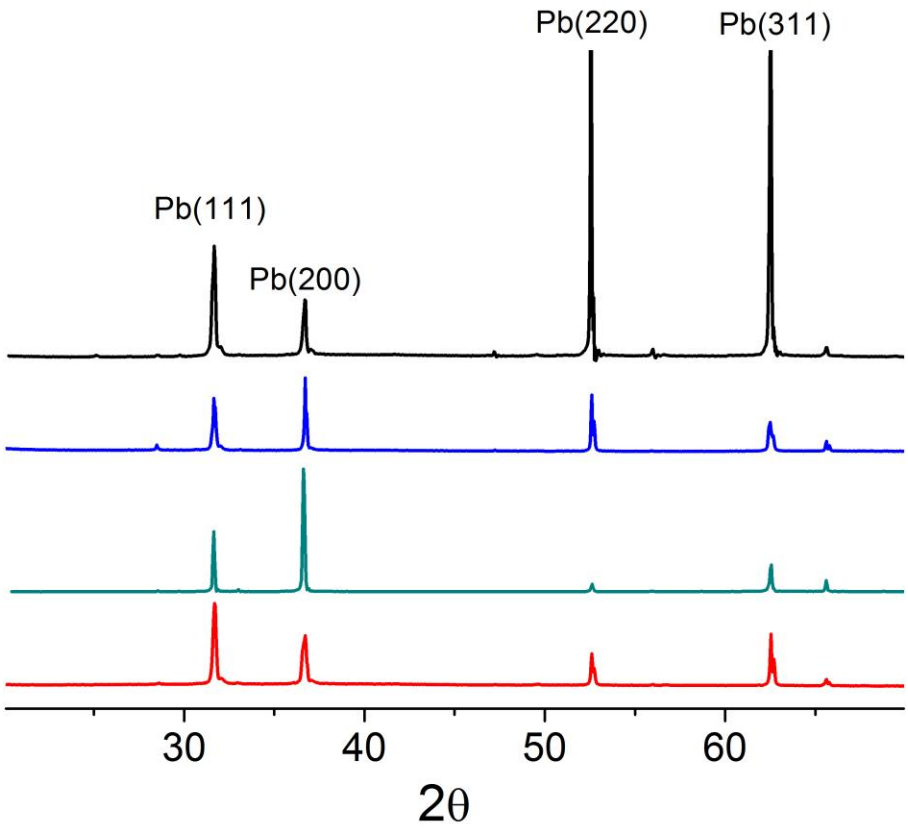

Figure 5. XRD patterns of four single treated od-Pb electrodes prepared in the same manner (*i.e.*, thermal oxidation in air at 220 °C for 24 hours followed by electrochemical reduction at -3.34 V vs $Cc^{0/+}$ for 4 hours).

The existence of metastable surface species on od-Pb can also be ruled out, based on results from FTAC voltammetry. Nonlinear harmonic components of FTAC voltammetry resulted from a large amplitude ac perturbation are sensitive to the underlying electron transfer processes associated with catalytically active sites hence allow these processes to be detected under catalytic turnover conditions.[18a] In previous studies, we have employed this technique to probe metastable active sites present on the electrode surface during oxidative water splitting. [24]

In order to investigate whether metastable active sites play an important role in electro-catalysis with od-Pb, FTAC voltammetry measurements were undertaken using untreated Pb, and single/double treated od-Pb electrodes. The results are shown in Figure 6(a), 6(b) and 6(c), respectively. Although nonlinear second and third harmonics are evident in the power spectrum for each sample, the lack of any

discernible faradaic process in the third harmonic in the current-potential data indicates that no metastable active sites exist on the single or double treated od-Pb electrodes. Notably, analysis of the first harmonic indicates that the non-faradaic (capacitance) current increases with each thermal oxidation/electrochemical reduction cycle. For example, at an applied potential of -0.4 V vs $Cc^{0/+}$, the measured current from the first harmonic of the untreated Pb, single treated od-Pb and double treated od-Pb electrodes is 0.26 mA cm^{-2}, 1.26 mA cm^{-2} and 2.71 mA cm^{-2}, respectively, meaning that the capacitance current of the single treated and double treated od-Pb electrodes is approximately 4.8 and 10.4 times higher than the untreated Pb electrode. This increase in capacitance current is attributed to an increase in the electroactive surface area of the porous od-Pb electrodes.

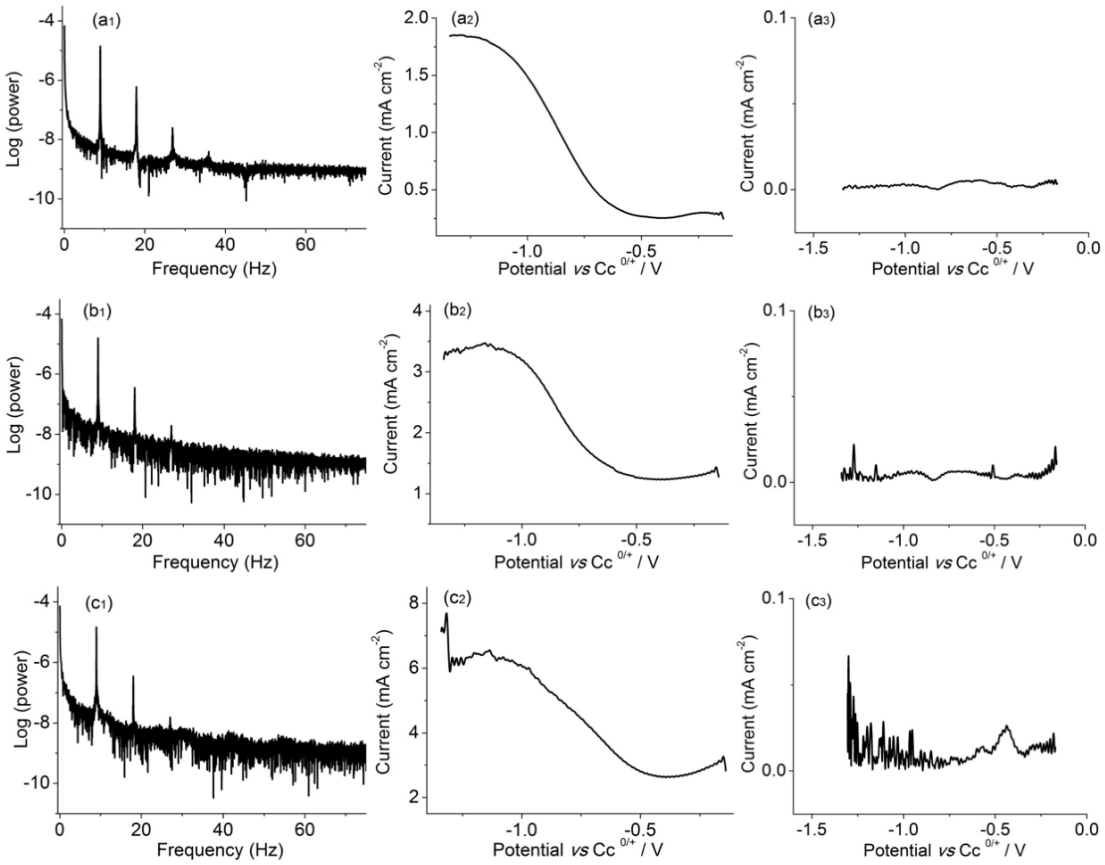

Figure 6. FTAC voltammetric data collected with (a) untreated Pb, (b) single treated od-Pb and (c) double treated od-Pb electrodes. Each group of data includes: (1) a power spectrum; (2) an envelope of the first harmonic and; (3) an envelope of the third harmonic

Based on the observations described above, the rougher surface produced during the formation of od-Pb that leads to a significantly increased electrochemically accessible surface area is thought to be the main contributor to the enhanced catalytic properties of this material. Indeed, Hall et. al. [21b] report that the significant enhancement in CO_2 reduction on od-Au electrodes originates from the generation of diffusional gradients within the pores of the meso-structured Au (200 nm pore diameter), rather than from changes to the surface crystallography or grain size. Sen et. al. [21a] also observe that CO_2 reduction products are highly dependent on the thickness of the surface layer on Cu 'foam' electrodes, again suggesting that mass

transport of the active species into the meso-structured electrode plays an important role. Finally, Dutta et. al. [25] reported that the transient trapping of gaseous intermediates inside meso-structured pores on Cu electrode during CO_2 electro-reduction has a significant influence on the selectivity of the electrolysis products.

All these studies highlight the influence that surface roughness and meso-structure have on the performance of heterogeneous electro-catalysts during CO_2 reduction. In this work, we propose that on flat, unmodified Pb electrodes, proton mass transport is sufficient to support the HER while the solution is vigorously stirred during bulk electrolysis. By contrast, the relatively uniform meso-structure of the od-Pb electrodes which contain pores with diameters of about 300 nm, (see Figure 3(f)), inhibits mass transport of the proton carrying species like $[Me_2NH_2]^+$ to the surface, which leads to surface depletion of the proton concentration. The HER is thereby suppressed. Importantly, significant local depletion of the proton concentration is not expected to affect the concentration of reactive CO_2 present within the porous structure because the kinetics of the reactions shown in Eqs. 1 and 2 are slow. This hypothesis is supported by the results collected on double treated od-Pb in dimcarb with mixing molar ratio of CO_2:DMA < 1:1.8. Under these conditions, the concentration of available protons is relatively high and H_2 is the sole product detected during bulk electrolysis (see Table 3). Comparing the data in Table 3 to those in Table 2 reveals that the concentration of available protons from species such as $[Me_2NH_2]^+$ in dimcarb, has a critical influence on the electrolysis product distribution obtained with od-Pb.

Rough metallic electrodes can also be prepared by using very negative deposition potentials so hydrogen is evolved as the metal is deposited.[26] Another test further support the hypothesis that the enhanced catalytic performance of od-Pb is related to increased surface porosity/roughness, a porous Pb electrode was

synthesised by hydrogen co-evolution assisted electro-deposition of Pb on a Pb substrate in dimcarb. As demonstrated from the SEM image shown in Figure 7(a), a uniform meso-porous Pb foam was obtained by potentiostatic deposition at – 2.84 V vs. $Cc^{+/0}$ for 1 hour in dimcarb containing 40 mM $PbCl_2$. The average pore size is *ca.* 200 μm and the deposited metal exhibits distinctly dendritic morphology. This morphology is obviously different to the nano-coralline morphology of od-Pb [compare Figure 7a with Figure 3(f)], but nonetheless possesses intrinsically high surface area and roughness.

Following deposition, the Pb foam was tested as a catalyst for CO_2 reduction by bulk electrolysis in dimcarb and a summary of the product distribution is shown in Table 4. Comparison of the data shown in Table 4 to our previous study [7] clearly demonstrates that the Pb foam has enhanced catalytic activity for CO_2 reduction compared to untreated Pb. Finally, it is also worth noting that compact, smooth electro-deposited Pb [micrograph shown in Figure 7(b)] which was deposited at -0.34 V vs $Cc^{0/+}$, where no H_2 is co-generated, has little catalytic activity for CO_2 reduction in dimcarb. The FE for H_2 generation on this surface is 87% at an applied potential of -1.34 V vs $Cc^{0/+}$. Consequently, the surface roughness of lead electrodes plays a crucial role in the catalysis of CO_2 reduction in dimcarb.

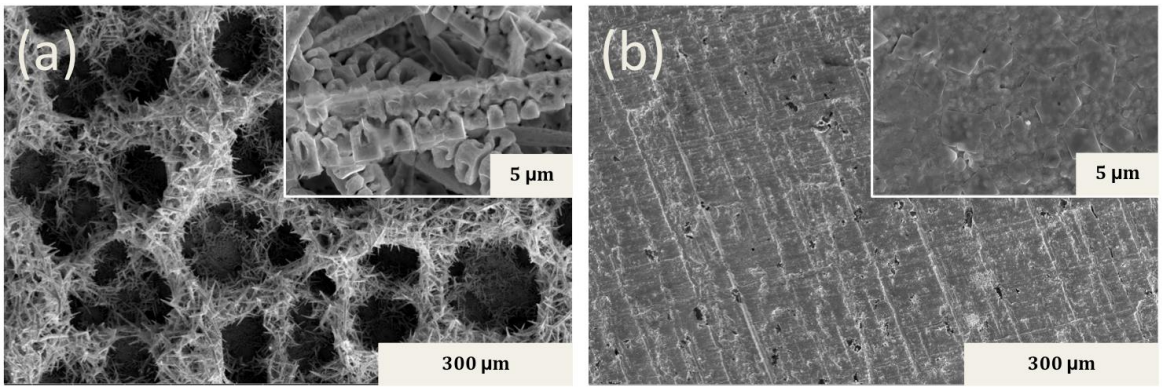

Figure 7. SEM image of electro-deposited Pb on flat Pb substrate, deposited in dimcarb containing 40 mM $PbCl_2$ by controlled constant potential deposition method with different deposition parameters: (a) -2.84 V vs. $Cc^{+/0}$, 1 hour (Pb foam) and; (b) -0.34 V vs. $Cc^{+/0}$, 1 hour (smooth Pb).

Table 4. Summary of product distribution after bulk electrolysis at different potentials with an electrodeposited Pb foam electrode in dimcarb.

Potential / V	Faradaic Efficiency			
	H_2	CO	$[HCOO]^-$	Sum
-1.34	47.6%	3.6%	45.0%	96.2%
-1.84	52.2%	6.4%	40.6%	99.2%
-2.34	53.1%	4.0%	42.6%	99.7%
-2.84	42.1%	7.0%	49.3%	98.4%
-3.34	53.6%	4.6%	40.6%	98.8%

Conclusions

The electro-catalytic performance of od-Pb electrodes for electro-reduction of CO_2 in dimcarb was investigated. Compared with an unmodified polycrystalline Pb electrode, where H_2 is the dominant electrolysis product (> 95%), od-Pb has been shown to be an effective electro-catalyst for CO_2 reduction in dimcarb with a mixing molar ratio of CO_2:DMA > 1:1.8. On this surface the faradaic efficiencies for the generation of H_2, CO and $[HCOO]^-$ were 15%, 10% and 75% respectively, and these efficiencies were invariant across a wide range of applied potentials. Analysis of the od-Pb by scanning electron microscopy and powder X-ray diffraction reveals that the

significant enhancement in catalytic activity over smooth and compact Pb surfaces originates from the increased surface roughness and greater surface area (ca. 10 times higher), rather than the existence of residual metal oxides, preferred crystal orientation or other metastable active sites.

Perhaps one of the most valuable outcomes of this work is that since the enhanced catalytic properties of od-Pb electrode originates from increased surface roughness rather than from the 'metal oxide-derived' process, the precursor to generate the functional catalyst is not restricted to metal oxides. Indeed, metal halides, metal carbonates and metal hydroxides could also be explored as precursors to generate structured metallic catalysts for CO_2 reduction applications. This is a topic to be explored in future work, in addition to physically and/or chemically doping the existing od-Pb catalysts with other metals such as Pd, Au, or Ag to reduce the CO_2 reduction overpotential, while maintaining the product selectivity.

Acknowledgments

L. C. acknowledges Monash University for provision of postgraduate scholarship support. The authors also gratefully acknowledge funding provided by Monash University through the Interdisciplinary Research Support Programs and use of the facilities available within the Monash X-ray Platform and the Monash Centre for Electron Spectroscopy.

Key words

Carbon Dioxide, Oxide Derived Catalyst, Electro-catalysis, Electrochemical Reduction

References

[1] a) J. S. Sawyer, *Nature* **1972**, *239*, 23-26; b) D. P. Schrag, *science* **2007**, *315*, 812-813.

[2] a) C. Costentin, M. Robert, J.-M. Savéant, *Chem. Soc. Rev.* **2013**, *42*, 2423-2436; b) J. Qiao, Y. Liu, F. Hong, J. Zhang, *Chem. Soc. Rev.* **2014**, *43*, 631-675.

[3] a) Q. Lu, J. Rosen, F. Jiao, *ChemCatChem* **2015**, *7*, 38-47; b) J. D. Watkins, A. B. Bocarsly, *ChemSusChem* **2014**, *7*, 284-290; c) B. A. Rosen, A. Salehi-Khojin, M. R. Thorson, W. Zhu, D. T. Whipple, P. J. Kenis, R. I. Masel, *Science* **2011**, *334*, 643-644; d) Y. Hori, in *Mod. Aspect. Electroc.* (Ed.: C. Vayenas), Springer, New York, **2008**, pp. 89-189.

[4] M. Bevilacqua, J. Filippi, H. A. Miller, F. Vizza, *Energy Technology* **2015**, *3*, 197-210.

[5] Y. Oh, H. Vrubel, S. Guidoux, X. Hu, *Chem Commun (Camb)* **2014**, *50*, 3878-3881.

[6] a) N. Hollingsworth, S. F. R. Taylor, M. T. Galante, J. Jacquemin, C. Longo, K. B. Holt, N. H. De Leeuw, C. Hardacre, *Angew. Chem. Int. Ed.* **2015**, *54*, 14164-14168; b) M. Alvarez-Guerra, J. Albo, E. Alvarez-Guerra, A. Irabien, *Energy Environ. Sci.* **2015**, *8*, 2574-2599; c) Q. He, J. W. O'Brien, K. A. Kitselman, L. E. Tompkins, G. C. T. Curtis, F. M. Kerton, *Catal. Sci. Technolog.* **2014**, *4*, 1513-1528; d) B.-H. Xu, J.-Q. Wang, J. Sun, Y. Huang, J.-P. Zhang, X.-P. Zhang, S.-J. Zhang, *Green Chem.* **2015**, *17*, 108-122.

[7] L. Chen, S. X. Guo, F. Li, C. Bentley, M. Horne, A. M. Bond, J. Zhang, *ChemSusChem* **2016**, *9*, 1271-1278.

[8] U. P. Kreher, A. E. Rosamilia, C. L. Raston, J. L. Scott, C. R. Strauss, *Molecules* **2004**, *9*, 387-393.

[9] a) C. W. Li, M. W. Kanan, *J. Am. Chem. Soc.* **2012**, *134*, 7231-7234; b) D. Ren, Y. Deng, A. D. Handoko, C. S. Chen, S. Malkhandi, B. S. Yeo, *ACS Catal.* **2015**, *5*, 2814-2821; c) K. W. Frese, *J. Electrochem. Soc.* **1991**, *138*, 3338-3344.

[10] Y. Chen, C. W. Li, M. W. Kanan, *J. Am. Chem. Soc.* **2012**, *134*, 19969-19972.

[11] a) Y. Chen, M. W. Kanan, *J. Am. Chem. Soc.* **2012**, *134*, 1986-1989; b) R. Zhang, W. Lv, L. Lei, *Appl. Surf. Sci.* **2015**, *356*, 24-29; c) R. Shiratsuchi, K. Hongo, G. Nogami, *J. Electrochem. Soc.* **1992**, *139*, 2544-2549.

[12] C. H. Lee, M. W. Kanan, *ACS Catal.* **2015**, *5*, 465-469.

[13] J. Rosen, G. S. Hutchings, Q. Lu, S. Rivera, Y. Zhou, D. G. Vlachos, F. Jiao, *ACS Catal.* **2015**, *5*, 4293-4299.

[14] S. Zhang, P. Kang, T. J. Meyer, *J. Am. Chem. Soc.* **2014**, *136*, 1734-1737.

[15] a) S. Gao, Y. Lin, X. Jiao, Y. Sun, Q. Luo, W. Zhang, D. Li, J. Yang, Y. Xie, *Nature* **2016**, *529*, 68-71; b) S. Gao, X. Jiao, Z. Sun, W. Zhang, Y. Sun, C. Wang, Q. Hu, X. Zu, F. Yang, S. Yang, L. Liang, J. Wu, Y. Xie, *Angew. Chem. Int. Ed. Engl.* **2016**, *55*, 698-702.

[16] a) A. I. Bhatt, A. M. Bond, *J. Electroanal. Chem.* **2008**, *619-620*, 1-10; b) A. I. Bhatt, A. M. Bond, J. Zhang, *J. Solid State Electrochem.* **2006**, *11*, 1593-1603; c) A. I. Bhatt, A. M. Bond, D. R. MacFarlane, J. Zhang, J. L. Scott, C. R. Strauss, P. I. Iotov, S. V. Kalcheva, *Green Chem.* **2006**, *8*, 161-171.

[17] A. M. Bond, N. W. Duffy, S. X. Guo, J. Zhang, D. Elton, *Anal. Chem.* **2005**, *77*, 186A-195A.

[18] a) S. X. Guo, A. M. Bond, J. Zhang, *Rev. Polarogr.* **2015**, *61*, 21-32; b) A. M. Bond, D. Elton, S. X. Guo, G. F. Kennedy, E. Mashkina, A. N. Simonov, J. Zhang, *Electrochem. Commun.* **2015**, *57*, 78-83.
[19] L. E. Barrosse-Antle, A. M. Bond, R. G. Compton, A. M. O'Mahony, E. I. Rogers, D. S. Silvester, *Chem. Asian J.* **2010**, *5*, 202-230.
[20] A. Fromhold Jr, in *Theory of metal oxidation, Vol. 2*, North-Holland Publ. Co, Netherlands, **1980**.
[21] a) S. Sen, D. Liu, G. T. R. Palmore, *ACS Catal.* **2014**, *4*, 3091-3095; b) A. S. Hall, Y. Yoon, A. Wuttig, Y. Surendranath, *J. Am. Chem. Soc.* **2015**, *137*, 14834-14837.
[22] a) K. W. Frese, *J. Electrochem. Soc.* **1991**, *138*, 3338-3344; b) M. Le, M. Ren, Z. Zhang, P. T. Sprunger, R. L. Kurtz, J. C. Flake, *J. Electrochem. Soc.* **2011**, *158*, E45-E49; c) R. Shiratsuchi, Y. Aikoh, G. Nogami, *J. Electrochem. Soc.* **1993**, *140*, 3479-3482; d) G. Nogami, H. Itagaki, R. Shiratsuchi, *J. Electrochem. Soc.* **1994**, *141*, 1138-1142; e) R. Shiratsuchi, K. Hongo, G. Nogami, S. Ishimaru, *J. Electrochem. Soc.* **1992**, *139*, 2544-2549; f) T. Y. Chang, R. M. Liang, P. W. Wu, J. Y. Chen, Y. C. Hsieh, *Mater. Lett.* **2009**, *63*, 1001-1003; g) J. L. Qiao, M. Y. Fan, Y. S. Fu, Z. Y. Bai, C. Y. Ma, Y. Y. Liu, X. D. Zhou, *Electrochim. Acta* **2015**, *153*, 559-565; h) T. Sekimoto, M. Deguchi, S. Yotsuhashi, Y. Yamada, T. Masui, A. Kuramata, S. Yamakoshi, *Electrochem. Commun.* **2014**, *43*, 95-97; i) S. M. Bashir, S. S. Hossain, S. U. Rahman, S. Ahmed, M. M. Hossain, *Electrocatalysis* **2015**, *6*, 544-553; j) V. S. K. Yadav, M. K. Purkait, *Rsc Advances* **2015**, *5*, 40414-40421; k) S. Ohya, S. Kaneco, H. Katsumata, T. Suzuki, K. Ohta, *Catal. Today* **2009**, *148*, 329-334; l) S. Lee, J. D. Ocon, Y. I. Son, J. Lee, *J. Phys. Chem. C* **2015**, *119*, 4884-4890; m) Y. C. Hsieh, S. D. Senanayake, Y. Zhang, W. Q. Xu, D. E. Polyansky, *ACS Catal.* **2015**, *5*, 5349-5356; n) D. Kim, S. Lee, J. D. Ocon, B. Jeong, J. K. Lee, J. Lee, *Phys. Chem. Chem. Phys.* **2015**, *17*, 824-830.
[23] a) Z. Wang, G. Yang, Z. Zhang, M. Jin, Y. Yin, *Acs Nano* **2016**, *10*, 4559-4564; b) R. Kas, R. Kortlever, A. Milbrat, M. T. Koper, G. Mul, J. Baltrusaitis, *Phys. Chem. Chem. Phys.* **2014**, *16*, 12194-12201; c) H. Zhang, Y. Ma, F. Quan, J. Huang, F. Jia, L. Zhang, *Electrochem. Commun.* **2014**, *46*, 63-66; d) L. Q. Zhou, C. Ling, M. Jones, H. Jia, *Chem. Commun.* **2015**, *51*, 17704-17707.
[24] Y. Liu, S. X. Guo, A. M. Bond, J. Zhang, Y. V. Geletii, C. L. Hill, *Inorg. Chem.* **2013**, *52*, 11986-11996.
[25] A. Dutta, M. Rahaman, N. C. Luedi, M. Mohos, P. Broekmann, *ACS Catal.* **2016**, *6*, 3804-3814.
[26] a) H. C. Shin, J. Dong, M. Liu, *Adv. Mater.* **2003**, *15*, 1610-1614; b) B. J. Plowman, L. A. Jones, S. K. Bhargava, *Chem. Commun.* **2015**, *51*, 4331-4346.

Electrochemical Reduction of CO_2 with an Oxide Derived Lead Nano-Coralline Electrode in the Distillable Ionic Liquid, Dimcarb

Lu Chen,[a] Fengwang Li,[a] Cameron Bentley,[b] Mike Horne,[c]

Alan M. Bond,[a] and Jie Zhang*[a]

[a]School of Chemistry and ARC Centre of Excellence for Electromaterials Science, Monash University, Clayton, Vic 3800, Australia

[b]Department of Chemistry, University of Warwick, Coventry, CV4 7AL, U.K.

[c]CSIRO Minerals Resources Flagship, Clayton, Vic 3168, Australia

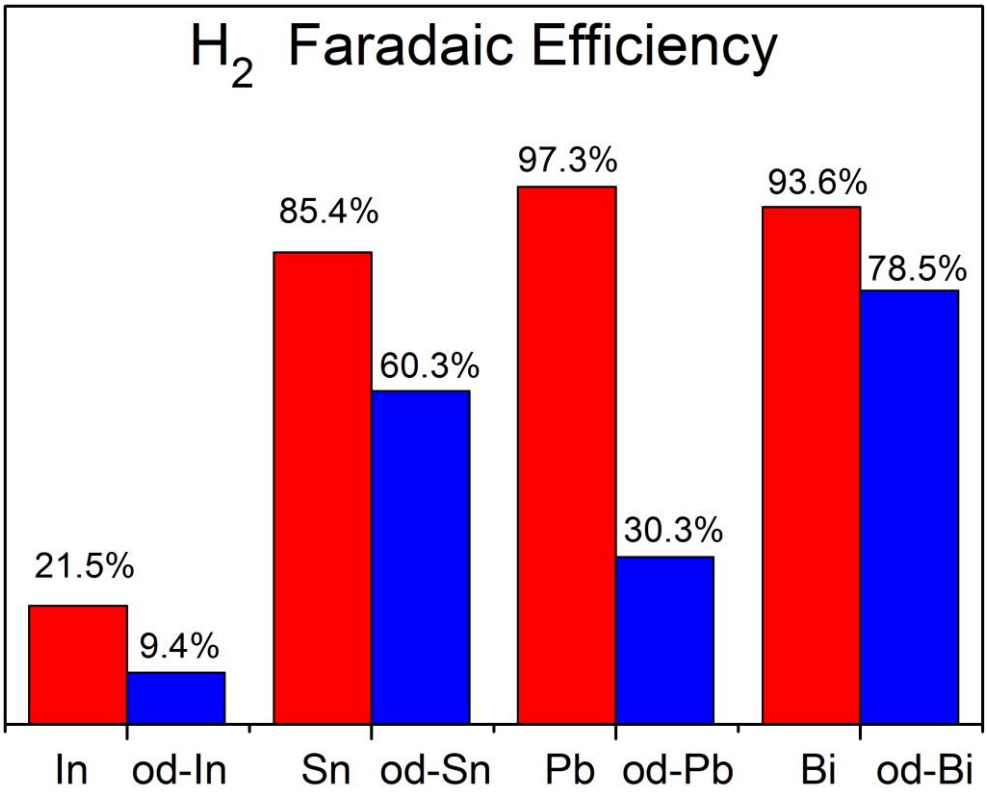

Figure S1. FEs for generation of H_2 calculated for each metal samples from analysis of the electrolysis products after bulk electrolysis in dimcarb at an applied potential of -1.34 V vs. $Cc^{+/0}$.